# Biophysics and protein corona analysis of Janus cyclodextrin-DNA nanocomplexes. Efficient cellular transfection on cancer cells

M. Martínez-Negro[a], G. Caracciolo[b], S. Palchetti[b], D. Pozzi[b], A. L. Capriotti[c], C. Cavaliere[c], A. Laganà[c], C. Ortiz Mellet[d], J. M. Benito[e], J. M. García Fernández[e], E. Aicart[a], E. Junquera[a,*]

[a]Grupo de Química Coloidal y Supramolecular, Departamento de Química Física I, Facultad de Ciencias Químicas, Universidad Complutense de Madrid, 28040-Madrid, Spain

[b]Department of Molecular Medicine, "Sapienza" University of Rome, Viale Regina Elena 291, 00161-Rome, Italy

[c]Department of Chemistry, "La Sapienza" University of Rome, Pzle Aldo Moro 5, 00185-Rome, Italy

[d]Departamento de Química Orgánica, Facultad de Química, Universidad de Sevilla, c/ Profesor García González 1, 41012-Sevilla, Spain

[e]Instituto de Investigaciones Químicas (IIQ), CSIC – Universidad de Sevilla, Avda. Américo Vespucio 49, 41092-Sevilla, Spain

Corresponding Author

*Fax: +34913944135. E-mail: junquera@quim.ucm.es

**ABSTRACT**

The self-assembling processes underlining the capabilities of facially differentiated ("Janus") polycationic amphiphilic cyclodextrins (paCDs) as non-viral gene nanocarriers have been investigated by a pluridisciplinary approach. Three representative Janus paCDs bearing a common tetradecahexanoyl multitail domain at the secondary face and differing in the topology of the cluster of amino groups at the primary side were selected for this study. All of them compact pEGFP-C3 plasmid DNA and promote transfection in HeLa and MCF-7 cells, both in absence and in presence of human serum. The electrochemical and structural characteristics of the paCD-pDNA complexes (CDplexes) have been studied by using zeta potential, DLS, SAXS, and cryo-TEM. paCDs and pDNA, when assembled in CDplexes, render effective charges that are lower than the nominal ones. The CDplexes show a self-assembling pattern corresponding to multilamellar lyotropic liquid crystal phases, characterized by a lamellar stacking of bilayers of the CD-based vectors with anionic pDNA sandwiched among them. When exposed to human serum, either in the absence or in the presence of pDNA, the surface of the cationic CD-based vector becomes coated by a protein corona (PC) whose composition has been analysed by nanoLC-MS/MS. Some of the CDplexes herein studied showed moderate-to-high transfection levels in HeLa and MCF-7 cancer cells combined with moderate-to-high cell viabilities, as determined by FACS and MTT reduction assays. The ensemble of data provides a detail picture of the paCD-pDNA-PC association processes and a rational base to exploit the protein corona for targeted gene delivery on future *in vivo* applications.

**KEYWORDS:** CDplexes, effective charge ratio, multilamellar phases, cellular transfection, cytotoxicity, protein corona

## 1. Introduction

Nucleic acids (DNA or RNA) have become in the last decade an attractive source of therapeutic agents [1]. The interplay of a direct structure-activity relationship and a highly specific mode of action theoretically permit exploiting the cellular machinery in a predictable fashion to either stimulate or silence the expression of virtually any protein, with reduced toxicity and fewer side effects as compared with classical drugs. This is the basis of gene therapy (GT), an exciting branch of medicine that tries to cure diseases (genetic, neurologic, cardiovascular, infectious, or carcinogenic, etc.) at a molecular level, by repairing damaged cellular DNA, either by introducing (by means of a plasmid DNA) and expressing a copy of the affected or missing gene into the cells [2-8] or by inserting a small interfering RNA (siRNA) to silence and stop the expression of an abnormal gene, responsible of the cell disorder [9-12]. Both approaches, either that one based on plasmid DNAs or on siRNAs, constitute nowadays the main strategies of GT on seeking for effectively restore healthy cell functioning.

Conventional drugs consist of bioactive species and a carrier, the former being normally the key of the design strategies. However, in the case of biomolecular drugs, such as nucleic acids, the carrier becomes a decisive protagonist. In the free state, nucleic acids are easily degraded by nucleases in biological fluids [13,14], and their membrane-crossing abilities and cellular uptake are seriously limited by their negative charge, inherently large size, and rigidity [15]. Formulation with appropriate delivery systems is thus essential for nucleic acids to overcome the physiological barriers, reach the target in a fully functional form and carry out the designed therapeutic function. Viral gene vectors [16,17] were first developed towards this end due to their high effectiveness. Yet, the use of viral vectors bear inherent risks, including immunogenicity and oncogenicity, which has boosted research on the design, synthesis, and

characterization of non-viral carriers that may combine high transfection efficiencies with low cytotoxicity levels [18,19]. In addition, for *in vivo* applications, these vectors must remain stable in the presence of blood or serum and, ideally, should be amenable to surface decoration with selective groups in order to recognize the target cells. The majority of non-viral vector formulations on record are based on cationic lipids [19,20], polymers [21], nanoparticles [22], and polysaccharides [12,23]. More recently, gene delivery systems based on 3D molecular frameworks with precisely defined chemical structures, sizes, shape symmetry and functional group distributions have been developed [24-26]. Their intrinsic monodisperse character allows conducting systematic studies on the influence of vector modifications on the supramolecular interactions with nucleic acids and the consequences in transfection efficiencies [1].

Within the context of molecular gene vectors, facially differentiated ("Janus") macrocyclic entities [24,26,27], among which cyclodextrin (CD)-based derivatives are paradigmatic examples, have conquered a prominent position [28,29]. CDs are biocompatible cyclic oligosaccharides consisting of $\alpha$-1,4-linked glucopyranose units that define a cone-shape topology with well-differentiated faces. The Janus feature can be imparted by bidirectional functionalization with polycationic groups on one rim and hydrophobic chains on the opposite rim. Multihead-multitail polycationic amphiphilic CDs (paCDs) with self-assembling properties and biomimetic cell-membrane-crossing aptitudes, resembling both cationic lipids and cationic polymers, are thus accessed [30,31]. In the presence of nucleic acids, they spontaneously form well-defined supramolecular nanocomplexes (hereinafter referred to as CDplexes) where the gene material is protected from degradation by enzymatic agents. Analogously to the well-known lipoplexes and polyplexes [32], CDplexes can elicit cellular uptake in physiological media and promote transfection [30,31,33,34].

Whereas *in vitro* transfection of immortalized cultured cells can be generally conducted in serum-free medium, some *ex-vivo* and any *in vivo* GT protocol will imply exposing of the nucleic acid-entrapping nanosystems to other biomolecules present in biological fluids. Non-specific interactions with these biomolecules may then decisively affect their fate in a biological environment [35,36]. Indeed, once administered *in vivo*, the nanovectors are exposed to the biological fluids from which they adsorb proteins and other components, losing the bare vector identity to form a biologically active corona, known as the *protein corona* (PC) [37,38]. This PC plays an important role in both the cellular recognition [39] and cell-membrane crossing capabilities (internalization process) of the nanovector [40]. It has also a clear effect on its time of circulation in the blood, so that knowing the proteomic profile of the corona surrounding a gene vector is crucial to optimize the transfection process. For instance, certain proteins like opsonins and, specially, immunoglobulins, fibrinogen and complement proteins are recognized by the macrophages favoring the phagocytosis and the rapid clearance of the vector from the bloodstream. On the other hand, the adsorption of apolipoproteins and serum albumin (dyopsonins) promote prolonged blood circulation half-life [41]. Successful delivery of therapeutic genes into cells will therefore require not only a high control of the physical-chemical parameters of the vector and vector-DNA nanocomplex, such as effective charges, chemical composition, size and structure, but also a deep knowledge on their interaction with serum proteins, the composition of the resulting PC and its impact in transfection capabilities and toxicity. Notwithstanding, up to date, most studies in this field are centered on the PC that forms around inorganic and organic nanoparticles [40,42-44], with only a few investigations evaluating the PC adsorbed on vector-DNA complexes [45,46].

This work is specifically focused on the biophysical and biochemical characterization of Janus paCD-pDNA CDplexes and their protein corona fingerprints as a function of the molecular paCD vector topology. We have chosen three different paCD representatives with a β-cyclodextrin (βCD) core, namely compounds **ADM70**, **ADM105** and **PBO234** (Scheme 1). The three molecular vectors share a $C_7$-symmetrical skirt-type Janus architecture with a multitail lipophilic domain formed by fourteen hexanoyl groups that esterify the secondary hydroxyls, differing in the architecture of the multivalent cationic cluster installed at the primary positions. Thus, **ADM70** displays a dendritic presentation of fourteen primary amino groups, **ADM105** a linear arrangement of seven secondary and seven primary amino groups and **PBO234** a heptavalent cluster of primary amino groups. **ADM70** and **ADM105** additionally incorporate a belt of seven thiourea groups at the primary face branches. All these structural elements have been previously found to impart good DNA compaction abilities to molecular gene vectors as well as good transfection capabilities to the corresponding vector-DNA complexes *in cellulo* and *in vivo* [33,34]. We have first conducted a deep electrochemical and structural characterization of the bare nanovector and pDNA-loaded Janus paCD assemblies by using high precision experimental techniques including zeta potential, agarose gel electrophoresis, dynamic light scattering (DLS), small angle X-ray scattering (SAXS) and cryo-transmission electron microscopy (cryo-TEM). Given that what cells "see" and process in *in vivo* situation is not the bare complexes but the CDplexes-PC bioentity formed, we have evaluated the PC developed at the surface of CDplexes formulated with the three paCDs herein used when they interact with human plasma (HP), by means of nano liquid chromatography tandem mass spectrometry (nanoLC-MS/MS). Finally, transfection performances of the CDplexes and levels of cellular toxicity were further investigated *in vitro* by

fluorescence-activated cell sorting (FACS) and reduction of 3-(4,5-dymethylthiazol-2-y1)-2,5-diphenyl tetrazolium bromide (MTT assay), respectively. The final goal of this pluridisciplinary approach is obtaining a global picture of the optimal requirements for the preparation of the CDplexes, in an attempt of opening alternative trails that provide non-viral vectors with improved outputs of bioavailability and transfection efficiency (TE).

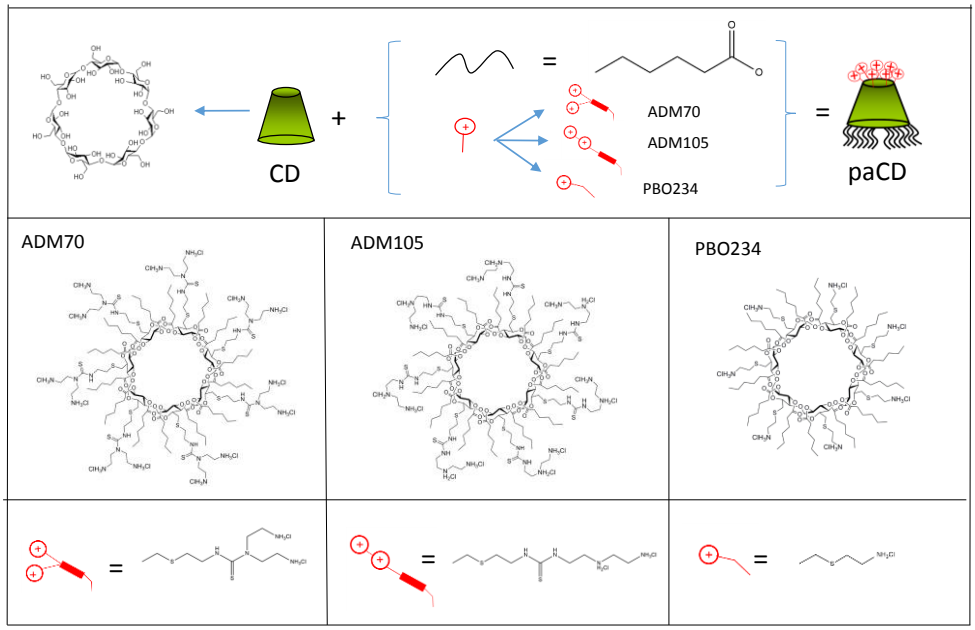


**Scheme 1.** Structural characteristics of ADM70, ADM105 and PBO234.

## 2. Experimental section

### 2.1 Materials

The Janus paCDs used in this study, **ADM70**, **ADM105** and **PBO234** (Scheme 1), were prepared following the procedures previously reported [47]. Briefly, the synthesis of compound **PBO234** was accomplished in four steps (i-iv) from commercially available β-cyclodextrin by (i) heptabromination at the primary hydroxyl rim with the N-bromosuccinimide (NBS)/triphenylphosphine (TPP) system [48], (ii) cesium carbonate promoted nucleophilic displacement of bromine by N-Boc-cysteamine [49],

(iii) acylation of the fourteen secondary hydroxyls by reaction with hexanoic anhydride in N,N-dimethylformamide (DMF) and N,N-dimethylaminopyridine (DMAP) as a non-nucleophilic base catalyst and (iv) final acid-promoted hydrolysis of the *tert*-butyl carbamate groups. Compounds **ADM105** and **ADM70** were obtained from **PBO234** after isothiocyanation of the seven amino groups with thiophosgene [47] followed by thiourea coupling reactions with mono-N-Boc-ethylenediamine or N,N"-di-Boc-ethylenetriamine, respectively, and subsequent Boc removal. The physicochemical data for the three polycationic amphiphilic cyclodextrins were consistent with those previously reported [47]. Most significantly, the $^{1}H$ and $^{13}C$ NMR spectra showed the typical single-spin system for fully $C_7$-symmetrical molecules.

pEGFP-C3 Plasmid DNA (pDNA) was extracted from competent *E. Coli* bacteria previously transformed with pEGFP-C3, the extraction being carried out using GenElute HP Select plasmid Gigaprep Kit (Sigma Aldrich) following a protocol previously described [50,51]. Sodium salt of calf thymus DNA (ctDNA), provided by Sigma-Aldrich, was used as linear DNA to determine the effective charge ( $q^{+}_{CD}$ ) of the cationic vector.

Human plasma (HP) whole blood provided by the Department of Experimental Medicine of La Sapienza University of Rome, was obtained by venipuncture of ten healthy volunteers. Mixed plasma was aliquoted and stored at -80 ºC in protein LoBind tubes until further use. For analysis, the aliquots were thawed at 4 ºC and then allowed to warm at room temperature. Human cervical cancer cell line (HeLa), derived from human cervix adenocarcinoma, and human breast cancer cell line (MCF-7), derived from human pleural effusion breast cancer metastasis, were purchase from ATCC (Manassas, VA, USA). HeLa cells were maintained in Eagle's Minimum Essential Medium (EMEM) supplemented with 2 mM L-glutamine, 100 IU/mL

penicillin/streptomycin, 1 mM sodium pyruvate, 10 mM HEPES, 1.5 mg/L sodium bicarbonate, and 10% fetal bovine serum (FBS). MCF-7 cells were maintained in Eagle's Minimum Essential Medium (EMEM) supplemented with 0.01 mg/ml human recombinant insulin and 10% fetal bovine serum (FBS).

## 2.2 Methods

**2.2.1 Preparation of CDplexes.** paCD-DNA complexes were formed by mixing the correct amounts of aqueous solutions of the paCDs and of DNAs (either ctDNA or pDNA) in HEPES 20 mM (pH = 7.4). The final solutions were left during 20 min prior to carry on the experiments. pDNA concentrations were optimized to fit the optimum conditions for each experimental technique. CDplex composition can be expressed either in terms of the masses ratio $\left(m_{CD} / m_{DNA}\right)_{\phi}$, between mass of the gene vector ( $m_{CD}$ ) to plasmid DNA $\left(m_{DNA}\right)$, or the effective charge ratio ($\rho_{eff}$), between the paCD and pDNA effective charges.

**2.2.2. Incubation of paCDs with HP, in absence and presence of pDNA.** paCDs were mixed with HP (1:1 v/v) and were incubated at 37 ºC for 1 h. After incubation, the samples were centrifuged three times during 15 min at 14000 rpm in order to wash the sample and remove all the molecules not bound to the complex. The same procedure was followed with the CDplexes.

**2.2.3. Methods for the characterization of paCD/pDNA CDplexes.** Uncomplexed plasmid DNA along with the paCD/pDNA CDplexes (at several $\left(m_{CD} / m_{pDNA}\right)$ ratios) were loaded onto 1% agarose gel and run for 30 min at 100 mV in 1x TAE (Tris-HCl, Acetate and EDTA) buffer. In the Agarose gel electrophoresis experiments, fully paCD/pDNA complexes appeared as fluorescent band in the wells of the gel, while

uncomplexed pDNA appeared outside the well. Fluorescence intensity of each band was measured by using commercial Quantity One software provided with Gel Doc XR instrument (Bio-Rad). The band intensity for the free pDNA was considered as 100% and other intensities were estimated accordingly.

ζ-potential measurements (obtained from electrophoretic mobility) for bare CDplexes were carried out at 25 ºC, with a Phase Analysis Light Scattering technique (Zeta PALS, Brookhaven Instrum. Corp., USA) [52,53]. ζ-Potential was measured at different $\left(m_{CD} / m_{DNA}\right)$ ratios of the CDplexes. Each electrophoretic mobility datum is taken as an average over 50 independent measurements. Size and ζ-potential measurements for PC-coated CDplexes (in the presence of HP) were carried out using a Zetasizer Nano ZS90 (Malvern, UK). CDplex-HP samples (1:1 volume ratio) were previously incubated for 1h at 37 ºC. CDplex-protein complexes were separated from excess plasma by centrifugation and extensive washing to remove the unbound proteins. For all of the samples investigated, the data show mostly a unimodal distribution and represent the average of at least five different measurements carried out for each sample. Results are given as means ± standard deviation of the five replicates.

Small-angle X-ray scattering (SAXS) experiments were carried out on the beamline NCD11 at ALBA Synchrotron Barcelona (Spain). The energy of the incident beam was 12.6 KeV ($\lambda$ = 0.995 Å). The machine is run in multibunch mode with a filling pattern consisting on 10 trains, 64 ns long and a gap of 24 ns between the trains. Samples were placed in sealed glass capillaries purchased from Hilgenberg with an outside diameter of 1.5 mm and wall thickness of 0.01 mm. The scattered X-ray was detected on CCD detector Quantum 210r, converted to one-dimensional scattering by radial averaging, and represented as a function of the momentum transfer vector. SAXS experiments were run, at several effective charge ratios ($\rho_{eff}$) of the CDplexes.

Cryo-transmission electron microscopy (Cryo-TEM) experiments were run for paCD/pDNA CDplexes following the standard procedure [54,55]. In these experiments, perforated Quantifoil R1.2/1.3 (hole diameter 1.2 μm) on a 400-mesh copper grid were used. Images were obtained using a Jeol JEM 2011 cryo-electron microscope operated at 200 kV, under low-dose conditions, and using different degrees of defocus (500–700 nm) to obtain an adequate phase contrast [56]. Images were recorded on a Gatan 794 Multiscan digital camera. Finally, the CCD images were processed and analyzed with a Digital Micrograph.

In order to carry on nanoLC-MS/MS analysis, 10 $\mu$L peptide mixtures were separated by RP chromatography using the Dionex Ultimate 3000 (Dionex Corporation Sunnyvale, CA, USA). Samples were on-line preconcentrated on a $\mu$-precolumn (Dionex, 300 $\mu$mi d. × 5 mm Acclaim PepMap 100 C18, 5 $\mu$m particle size, 100 Å pore size), employing a premixed mobile phase doubled distilled (dd) $H_2O$:ACN 98:2 (v/v) containing 0.1% (v/v) TFA at a flow-rate of 10 $\mu$L $min^{-1}$. Samples were then separated on an in-house manufactured Acclaim-C18 2.2 $\mu$m silica microparticles (75 $\mu$mi d. × 25 cm) and outlet Kasil frit. A multi-step gradient was employed for sample chromatography, using dd$H_2O$:ACN (98:2, v/v) with 0.1% TFA as phase A and ACN/TFA (99.9/0.1, v/v) as phase B. Starting from 1% phase B, such composition was maintained for 5 min, then phase B was linearly increased to 5% within 2 min; afterwards, phase B was first increased to 20% within 100 min and then to 50% within 43 min; then to 80% within the following 5 min. Phase B was maintained at 80% for 20 min to rinse the column and finally lowered to 1% within 1 min. The column was then equilibrated at this percentage for 43 min. The flow rate was 250 nL $min^{-1}$ and the total run time was 120 min. The nanoHPLC apparatus was directly connected with an Orbitrap Elite hybrid ion trap-Orbitrap mass spectrometer (Thermo Scientific, Bremen,

Germany) by a nano-electrospray ion source for MS/MS analysis of eluting peptides. Orbitrap Elite was operated to collect spectra over them/z range of 400–1800 Da, at 60,000 (Full Width Half Maximum at m/z 400) resolution, in the data dependent mode. MS/MS spectra were collected in top 20 mode, rejecting +1 and unassigned charge states, using a normalized collision energy of 35%, and an isolation window of 2 m/z. Ion trap and Orbitrap maximum ion injection times were set to 100 and 200 ms, respectively. Automatic gain control was used to prevent overfilling of the ion traps and was set to 1 × 106 for full FTMS scan, and 1 × 104 ions in MSn mode for the linear ion trap. To minimize redundant spectral acquisitions, dynamic exclusion was enabled with a repeat count of 1 and a repeat duration of 30 s with exclusion duration of 70 s. For each sample, three technical replicates (LC-MS/MS runs) were performed.

For data analysis and protein validation procedures, raw data files, obtained from Xcalibur software, were submitted to Proteome Discoverer (1.2 version, Thermo Scientific) for database search using Mascot (version 2.3.2 Matrix Science). Data were searched against human entries in the SwissProt protein database (57.15 version, 20266 sequences) selecting the built-in decoy option. Trypsin was specified as the proteolytic enzyme with up to two missed cleavages. Carbamidomethylation of cysteine and oxidation of methionine were set as fixed and variable modification, respectively. The monoisotopic mass tolerance for precursor ions and fragmentation ions were set to 10 ppm and 0.8 Da, respectively. To validate protein identifications derived from MS/MS sequencing results, the Mascot output files (.dat) were submitted in the commercial software Scaffold (v3.1.2, Proteome Software, Portland, Oregon, USA; http://www.proteomesoftware.com/). The scaffold tool to integrate Mascot identification results with X!Tandem search engine results (performed in automatic with the same parameters settled for Mascot) was used. Only protein identification based on

mass spectra correlating to at least two unique tryptic peptides were considered; minimum peptide identification probability was set at 95%, whereas protein identification probability was set at 99%. For protein quantitative analysis, Scaffold software allows the normalization of the spectral countings (normalized spectral countings, NSCs) and offers various statistical tests to identify significant abundance differences in two or more categories. The mean value of NSCs obtained in the three experimental replicates for each protein was further normalized to the protein molecular weight (MWNSC) and expressed as the relative protein quantity by applying Eq. (1):

$$MWNSC = \frac{(NSC / MW)}{\sum_{i=1}^{N}(NSC / MW)}100 \quad (1)$$

where MWNSCk is the percentage molecular weight normalized NSC for protein k, and MW is the molecular weight in kDa for protein k. This correction takes into account the protein size and evaluates the actual contribution of each protein reflecting its relative protein abundance (RPA) in the "hard corona".

On transfection efficiency analysis, HeLa and MCF-7 cells were seeded in 12-well plate ($150x10^3$ cells/mL) and treated with paCD/GFP plasmid complexes alone or surrounded by protein corona for 48 h. Then, cells were detached with trypsin/EDTA, washed two times with cold PBS and acquired using a flow cytometer. Fluorescence-activated cell sorting (FACS) analysis was performed using BD LSRFortessa equipped with 488 nm laser and with DIVA software (BD Biosciences, San Jose, CA, USA). Cells were first gated using forward *vs* side scatter (FSC vs SSC) strategy to exclude debris (low events) and then analyzed for the specific 530 nm emission (FITC channel). Data were analyzed using FlowJo software (FlowJo LLC data analysis software, Ashland, OR, USA). Transfection efficiencies (TE) were quantified by means of % GFP

cells, i.e., percentage of cells in which GFP expression is observed, and the average intensity of fluorescence per cell (MFI). Lipofectamine was used as a positive control.

Cell viability of HeLa and MCF-7 cell lines was assessed by 3-(4,5-dymethylthiazol-2-y1)-2,5-diphenyl tetrazolium bromide (MTT, mitochondrial respiration analysis; Sigma-Aldrich), according to Mosmann protocol. Briefly, HeLa and MCF-7 cells were seeded on 96-wells plate and, after 24 h, treated with the three paCDs (**ADM70**, **ADM105** and **PBO234**) complexed with pEGFP-C3 plasmid alone or surrounded by protein corona for 24 h. MTT was added to each well at the final concentration of 0.5 mg/mL and after 4 h of incubation at 37 ºC, the formazan salt was dissolved with 100 mL isopropanol. The absorbance of each well was measured with Glomax Discovery System (Promega) at 550 nm wavelength and the viability was calculated for each treatment as "OD of treated cells/OD of control cells" x100.

## 3. Results and discussion

Nanocomplex formation between non-viral gene vectors and nucleic acids is primarily driven by coulombic interactions. A proper characterization requires thus determination of the charges available in each partner, which are usually different from the nominal ones defined by the number of potentially ionizable groups. Regarding the oligonucleotide counterpart, studies reported in the literature [3,12,51,53] have shown that linear DNAs, such as commercial calf thymus or salmon sperm DNA, or short siRNAs have their negative charge totally available for the gene vector, i.e. $q^-_{linearDNA}$ = -2 per bp. In stark contrast, experiments recently reported [19,20,53] have demonstrated that, at physiological conditions, plasmid DNAs remain in a supercoiled conformation, rendering a much less negative charge than its nominal one ( $q^-_{pDNA}$ << -2).

For that reason, the characterization of the CDplexes must start with the determination of the effective charges of both the policationic Janus paCD and the pDNA, when forming the nanocomplex. At this respect, we have implemented a procedure to fulfil this objective based on a two-step protocol to determine: i) firstly, the effective charge of the cationic vector by characterizing the complex formed by this vector and double stranded linear DNA (linear DNA) for which the charge is well established (-2/bp); and ii) on a second step, the effective charge of the pDNA by characterizing the complex formed by the cationic vector, already of known charge (step i), and the pDNA in the same experimental conditions [51-53]. Briefly, the effective charge ratio ( $\rho_{eff}$ ), defined as the quotient between the effective charges of the paCD amino groups and the DNA phosphate groups is given by the following equation:

$$\rho_{eff} = \frac{n_+}{n_-} = \frac{q^+_{eff,CD}(m_{CD} / M_{CD})}{q^-_{eff,DNA}(m_{DNA} / \overline{M}_{bp})} \qquad (2)$$

where $n^+$ and $n^-$ are the number of moles of positive and negative charges of paCD and DNA; $m_{CD}$ and $m_{DNA}$ are the masses of the cationic CD based vector and the nucleic acid; $M_{CD}$ and $\overline{M}_{bp}$ are the molar mass of the vector and the average molar mass of DNA per bp; and $q^+_{eff,CD}$ and $q^-_{eff,DNA}$ are the effective charges of paCD and DNA per bp, respectively. When $n^+$ balances $n^-$, $\rho_{eff}$ equals 1 and the electroneutrality of the complex is reached. The particular $\left(m_{CD} / m_{DNA}\right)$ ratio at which this charge compensation occurs, defined hereinafter as $\left(m_{CD} / m_{DNA}\right)_{\phi}$, marks the lower limit from which the CDplex becomes a potentially efficient cell transfecting agent, since it turns to a net positively

charged complex, as required to cross the negative cell membrane in an efficient cell transfection process. From Eq. (2), it is easily deduced that $\rho_{eff}$ = 1 requires:

$$q^{+}_{eff,CD} = q^{-}_{eff,\text{linear}\,DNA}\left(\frac{m_{CD}}{m_{linearDNA}}\right)^{-1}_{\phi}\frac{M_{CD}}{\overline{M}_{bp}} \qquad (3)$$

Thus, if the isoneutrality ratio $\left(m_{CD}/m_{linearDNA}\right)_{\phi}$ is experimentally determined for a complex formed by a Janus CD-based vector and a commercial linear DNA (for which $q^{-}_{eff,\text{linear}\,DNA}$ = -2/bp), the effective positive charge of the vector ($q^{+}_{eff,CD}$) can be obtained. Once this charge is known, the negative effective charge of the plasmid ($q^{-}_{eff,\text{p}\,DNA}$) can be straightforwardly determined from the experimental value of $\left(m_{CD}/m_{pDNA}\right)_{\phi}$ for a complex formed by the same CD based vector but with a plasmid DNA instead of the linear DNA, on the same experimental conditions, as follows:

$$q^{-}_{eff,\text{p}\,DNA} = q^{+}_{eff,CD}\left(\frac{m_{CD}}{m_{pDNA}}\right)_{\phi}\frac{\overline{M}_{bp}}{M_{CD}} \qquad (4)$$

Electrochemical techniques are, among others, the most adequate tools to determine this electroneutrality ratio, agarose gel electrophoresis, and, more precisely, zeta potential, being the most recommended. Agarose gel electrophoresis informs about the compaction level of pDNA by the vectors. Fig.1 reports these experiments at three different $\left(m_{CD}/m_{DNA}\right)$ ratios (white numbers on lanes 2-4), for the three paCDs used in this work (**ADM70**, **ADM105** and **PBO234**). Uncomplexed pDNA (lane 1) was used as a positive control. Results reported in Fig. 1 reveal that pDNA is efficiently compacted by the paCD molecular vectors, since the fluorescent bands disappear across the gel lanes as long as $\left(m_{CD}/m_{DNA}\right)$ ratio increases. As can be inferred from Fig. 1, the

isoneutrality was reach at $\left(m_{CD} / m_{DNA}\right)$ ratios below 0.4, 0.7 and 0.5 for **ADM70**-pDNA, **ADM105**-pDNA and **PBO234**-pDNA CDplexes, respectively.

With the aim of determining with higher precision the electroneutrality ratio, zeta potential was measured as a function of $\left(m_{CD} / m_{DNA}\right)$ (Fig. 2), covering the range within which pDNA is effectively compacted by each paCD, according to the results shown in Fig. 1. The electroneutrality ratio $\left(m_{CD} / m_{DNA}\right)_{\phi}$ can be determined as the $\left(m_{CD} / m_{DNA}\right)$ value where a sign inversion on the charge occurs in the $\zeta$-potential sigmoidal profiles.

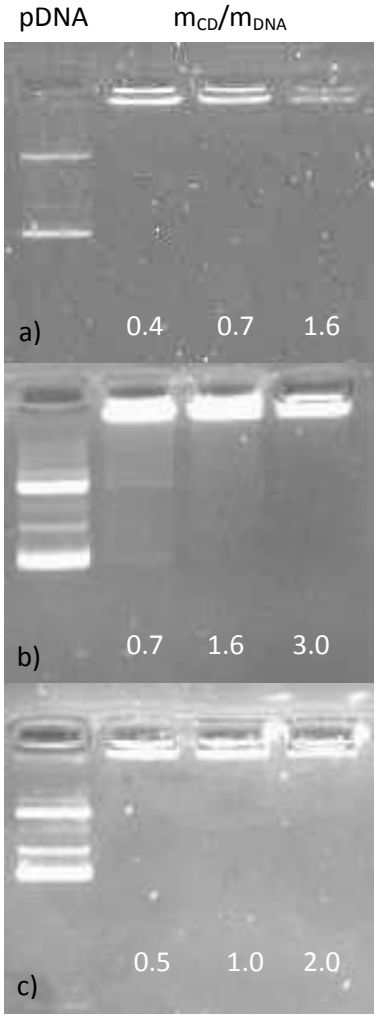


**Fig. 1.** Gel electrophoresis results for (a) **ADM70**-pDNA CDplexes, (b) **ADM105**-pDNA CDplexes, and (c) **PBO234**-pDNA CDplexes. Lane 1: uncomplexed pDNA (positive control). Lanes 2-4: CDplexes at different $m_{CD}/m_{DNA}$ mass ratios (white numbers at the bottom of the lanes).

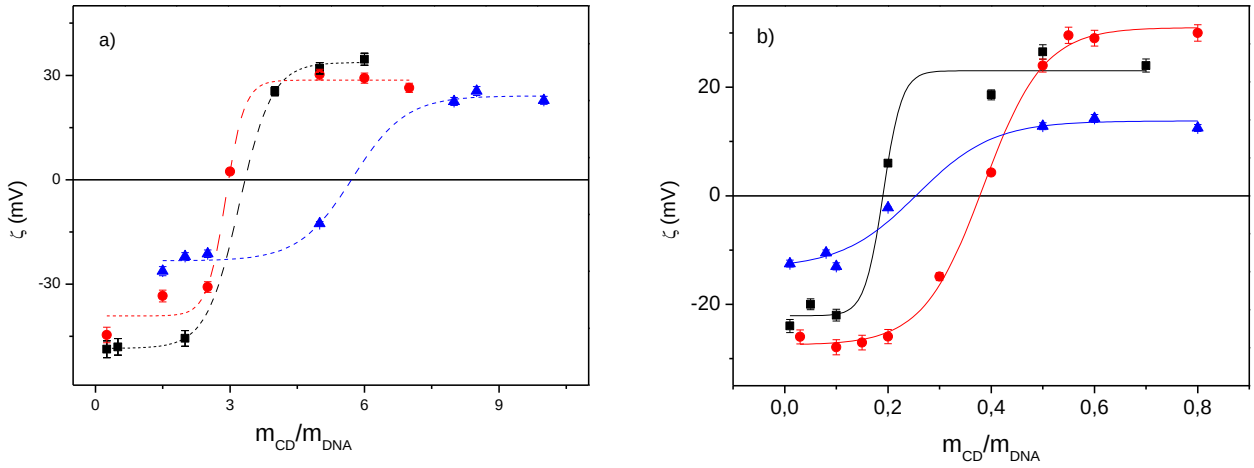


**Fig. 2.** Plot of $\zeta$ potential *vs* $m_{CD}/m_{DNA}$ CDplex composition, for different samples with ctDNA (a) and pDNA (b). Black, red and blue symbols correspond to **ADM70**-pDNA, **ADM105**-pDNA and **PBO234**-pDNA CDplexes, respectively.

Table 1 reports the results obtained for CDplexes formulated with **ADM70**, **ADM105** or **PBO234** and either ctDNA or pDNA. With these $\left(m_{CD} / m_{DNA}\right)_{\phi}$ values and following the procedure above explained, the effective charges of both the Janus CD based cationic vectors and the pDNA herein used, $q^{+}_{eff,CD}$ and $q^{-}_{eff,\mathrm{p}DNA}$, were calculated and collected in Table 2. The differences encountered between nominal and effective charges in both the cationic vectors and the anionic pDNA are remarkable. Thus, the net positive charges available for interaction with pDNA are around 33% of the nominal one, assuming full protonation of the amino groups, for the tetradecaamine derivatives **ADM70** and **ADM105**, and only 25% for heptamine **PBO234**. This scenario is similar to that found for some CD polyrotaxane-based vectors [12] but sharply different from that encountered for cationic lipid gene vectors bearing quaternary amino groups, which normally yield their total nominal positive charges within a range of 10 % of uncertainty [19,51,57]. On the other hand, the plasmid used herein seems to be quite supercoiled at the experimental conditions used, since its available negative charge per bp is far away from the nominal value (-2/bp), yielding

around 7%, 13% and 5% of its nominal charge when being compacted by **ADM70**, **ADM105** and **PBO234**, respectively. This behaviour, often found in lipoplexes, confirms that plasmids usually retain an important percentage of cationic sodium counter-ions ($Na^+$). This is *a priori* a favourable feature for the use of these macrocyclic vectors as safer and effective vehicles of nucleic acids, since the weaker the anionic character of the DNA, the lower the amount of cationic vector needed to formulate the nanocomplexes, thus decreasing the risk of cytotoxicity of the vector. From the paCD and pDNA effective charges thus obtained, effective charge ratios ($\rho_{eff}$) around 5-fold (for **ADM70** and **PBO234**) or 2- to 3-fold (for **ADM105**) of the nominal ones were calculated using Eq. (2).

**Table 1.** Values of isoneutrality ratios $\left(m_{CD} / m_{DNA}\right)_{\phi}$ for the CDplexes formed by ADM70, ADM105 and PBO234 with either ctDNA or pDNA.

| | **ADM70**-DNA | **ADM105**-DNA | **PBO234**-DNA |
|---|---|---|---|
| ctDNA | 3.0 | 2.9 | 5.7 |
| pDNA | 0.19 | 0.38 | 0.25 |

Values estimated with a 5% error

**Table 2.** Nominal and effective charges of paCDs and pDNA.

| | **ADM70** | **ADM105** | **PBO234** |
|---|---|---|---|
| $q^{+}_{nom,CD}$ | 14 | 14 | 7 |
| $q^{+}_{eff,CD}$ | 4.6 | 4.7 | 1.7 |
| $q^{+}_{eff,CD} / q^{+}_{nom,CD}$ | 0.33 | 0.33 | 0.25 |
| $q^{-}_{nom,pDNA} / bp$ | -2 | -2 | -2 |
| $q^{-}_{eff,pDNA} / bp$ | -0.13 | -0.26 | -0.09 |
| $q^{-}_{eff,pDNA} / q^{-}_{nom,pDNA}$ | 0.07 | 0.13 | 0.05 |
| $\rho_{eff}/\rho_{nom}$ | 5.1 | 2.6 | 5.4 |

Values estimated with an 8% error

Having information of the structure of the complex is important to find the best non-viral vectors and to promote its use in *in vivo* gene therapy. The structure of the paCD-pDNA CDplexes in concentrated samples was investigated by SAXS at several

effective charge ratios for which CDplexes are potentially active as gene transfection vectors ($\rho_{eff} > 1$). Cryo-TEM was also used as a supporting technique. Fig. 3 shows the corresponding SAXS diffractograms (Intensity *vs* $q$ factor) at $\rho_{eff} = 2$, 4 and 8, with the Miller indexes being included in the plot. In all the cases, three peaks that index well to a lamellar lyotropic liquid crystal phase ($L_\alpha$) were observed, regardless of $\rho_{eff}$, with the characteristic inter-layer distance ($d$) directly related to the $q$ factor ($d = 2\pi n/q_{hkl}$, $n$ is the diffraction order). This structure may be explained by considering that the hexanoyl chains linked to the wider entrance of the β–CD torus promote self-assembling in a lipidic bilayer fashion, CDplexes being adequately represented as alternating bilayers of paCDs molecules and an aqueous monolayer containing supercoiled pDNA, with thicknesses represented by $d_m$, and $d_w$, respectively, being $d = d_m + d_w$.

Table 3 collects the values of $d$, calculated as an average of the data obtained from the more intense peaks (100 and 200) of the diffractograms at each $\rho_{eff}$ ratio. It is noticeable that the periodicity of the structure remains basically unaltered for a constant pDNA content when the proportion of the vector increases (i.e. $d$ remains basically constant with $\rho_{eff}$), for the three CDplexes studied. Considering these $d$ values and the fact that pDNA supercoils needs around $d_w$ ~2.0-2.5 nm to be sandwiched by paCDs bilayers in a typical sandwich fashion, it can be deduced that the thickness of the bilayer ($d_m$) must be ~3.1, 3.4 and 2.5 nm for **ADM70-**pDNA, **ADM105**-pDNA and **PBO234-**pDNA CDplexes, respectively. Given the lengths of both the cationic tails and the lipid type chains, and the depth of the $\beta$-CD torus-shaped cavity, these $d$, $d_m$ and $d_w$ values are compatible with a $L_\alpha$ structure only if: i) the cationic tails on the narrower entrance of the CD macrocycle are somehow in an open bouquet fashion (to avoid electrostatic repulsions among positive charges) and/or ii) the lipidic type chains that are linked to the wider entrance of β-CD macrocycle are intercrossed.

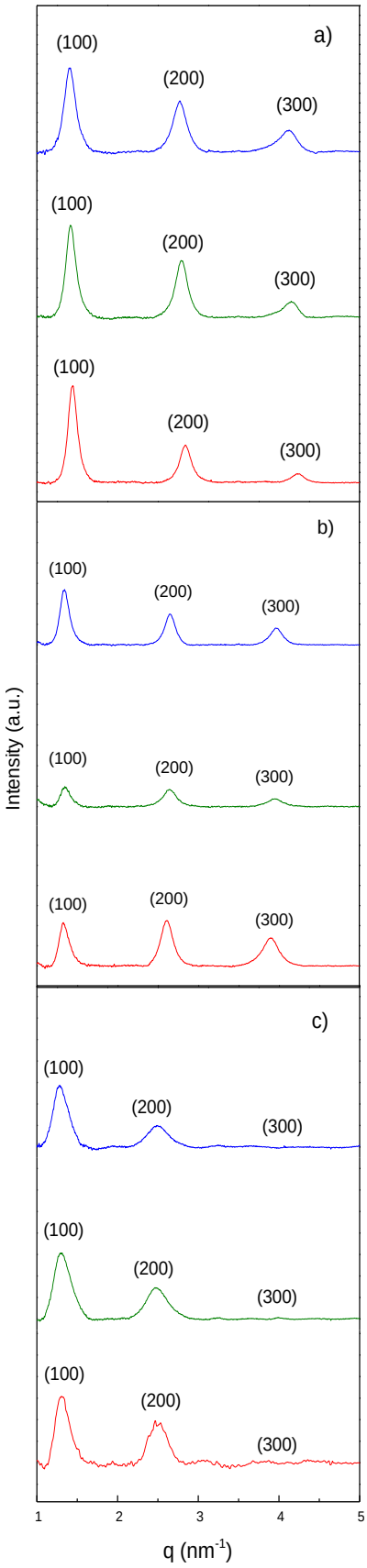


**Fig. 3.** SAXS diffractograms of paCD-pDNA CDplexes at several effective charge ratios ($\rho_{eff}$): Red lines $\rho_{eff}$ = 2, green lines $\rho_{eff}$ = 4, and blue lines $\rho_{eff}$ = 8 for: a) **ADM70**-pDNA; b) **ADM105**-pDNA; and c) **PBO234**-pDNA CDplexes.

**Table 3.** Values of $q$ and $d$ of the lamellar ($L_\alpha$) liquid crystal phase found for the paCD-pDNA CDplexes (where paCDs are ADM70, ADM105 and PBO234), at several effective charge ratios ($\rho_{\text{eff}}$).

| | | **ADM70** | **ADM105** | **PBO234** |
|---|---|---|---|---|
| $\rho_{eff}$ | | $L_\alpha$ | $L_\alpha$ | $L_\alpha$ |
| 2 | $q_{100}$ | 1.12 | 1.06 | 1.28 |
| | $q_{200}$ | 2.21 | 2.09 | 2.50 |
| | $q_{300}$ | 3.30 | 3.12 | - |
| | $d$ | 5.6 | 5.9 | 5.0 |
| 4 | $q_{100}$ | 1.13 | 1.09 | 1.31 |
| | $q_{200}$ | 2.23 | 2.13 | 2.47 |
| | $q_{300}$ | 3.33 | 3.16 | - |
| | $d$ | 5.6 | 5.8 | 5.0 |
| 8 | $q_{100}$ | 1.15 | 1.07 | 1.30 |
| | $q_{200}$ | 2.27 | 2.12 | 2.50 |
| | $q_{300}$ | 3.39 | 3.18 | - |
| | $d$ | 5.5 | 5.9 | 4.9 |

Values of $q$ and $d$ are reported in $nm^{-1}$ and nm, respectively.

Cryo-TEM experiments further confirmed the multilamellar character of the CDplexes studied in this work. Fig. 4 shows a selection of micrographs among those taken for **ADM105**-pDNA CDplex that are representative of the ensemble of data (see Fig. S1 in Supplementary data for a selection of micrographs of **ADM70**-pDNA and **PBO234**-pDNA CDplexes). The multilamellar arrangement found in SAXS is also seen in these micrographs. In fact, three types of nanostructures in coexistence are found: (i) CDplexes with a well-defined multilamellar profile and aggregated in a cluster type fashion (CT-type nanoaggregates; labelled with white asterisks in Fig. 4); (ii) CDplexes with a clear finger-print multilamellar pattern (FP-type nanoaggregates; labelled with white circles, and a zoom view in panel d), and; (iii) self-aggregated paCDs without pDNA compacted (labelled with white arrows), with a typical vesicle-type structure. The presence of aggregates of paCD molecules, without pDNA being compacted, is justified by the fact that the experiment is done for samples with a clear excess of cationic vector (notice that $\rho_{eff} = 4$ in cryo-TEM experiments). These exceeding paCD

molecules tend to form unilamellar spherical vesicle-type nanostructures, the formation of the lipidic bilayer being promoted by the presence of 14 lipidic type chains linked to the wider entrance of each cyclodextrin torus (2 chains per glucose unit). It can be inferred that the unilamellar paCD vesicles above mentioned interact with pDNA through strong electrostatic interactions and tend to aggregate yielding the multilamellar phases, either CT or FP, by sandwiching the plasmid supercoils within the aqueous monolayer that remain between each two bilayers. Scheme 2 shows schematic drawings of both nanoaggregates: (a) unilamellar vesicles in the absence of pDNA, and (b) multilamellar complexes in the presence of pDNA. In the CT-type structures, the bilayers may be deformed when sandwiching pDNA supercoils with the adjacent bilayers, but they essentially keep their morphologies. However, FP-type nanoaggregates show the typical finger-print compaction pattern, and in contrast with the CT-type CDplexes, the bilayers tend to disrupt probably due to a more favourable paCD-pDNA interaction. This particular scenario has been also previously found for different lipoplexes (cationic lipids-pDNA complexes) [20,57]. Some of the multilamellar arrangements shown in these micrographs (and other not shown) have been chosen to analyze the presence of periodicity. As representative examples, the insets of panels b) and c) in Fig. 4, show Fast Fourier Transform (FFT) profiles where the diffraction spot corresponds to a typical lamellar pattern.

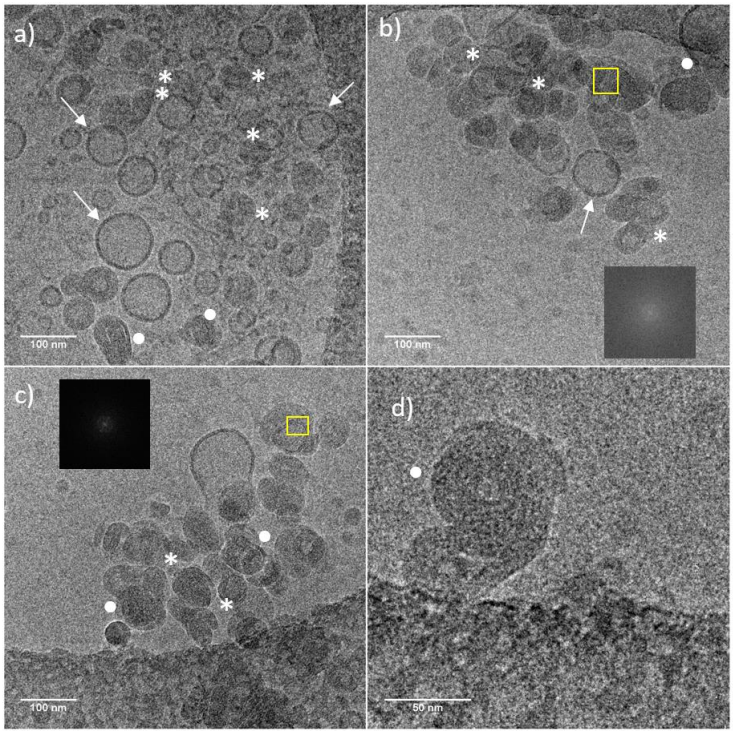


**Fig. 4.** A selection of cryo-TEM micrographs showing a general view of the **ADM105**-pDNA CDplexes at $\rho_{eff} = 4$. Insets on panels b) and c) show the diffraction spots from FFT calculations over a selected area on the original micrograph (yellow square). FFT pattern reveals a multilamellar structure. Scale bars are 100 nm in panels a-c and 50 nm in panel d.

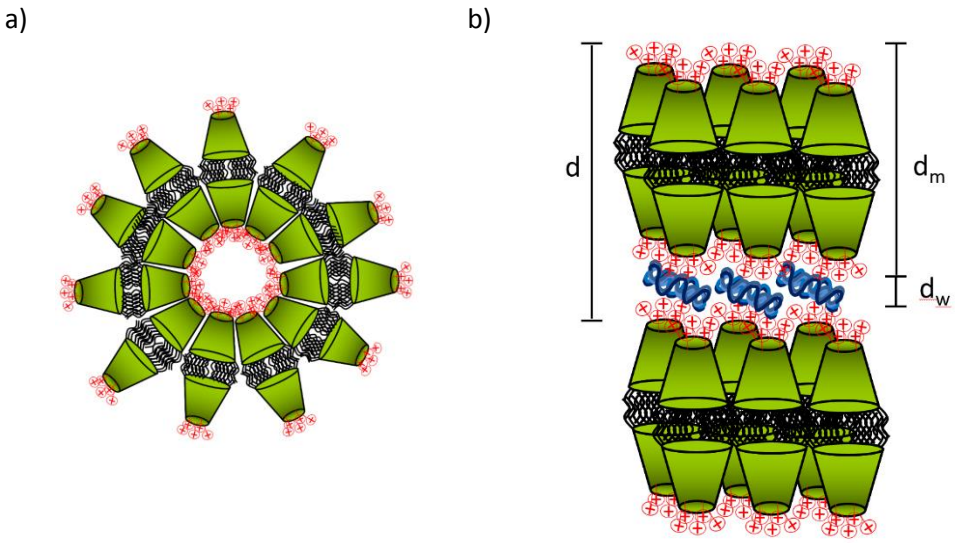


**Scheme 2.** Schematic drawings of: a) Vesicles-type paCD self-aggregation pattern; and b) Multilamellar lyotropic liquid crystal phase ($L_\alpha$) of the CDplexes studied in this work, showing the structural parameters, $d$, $d_m$ and $d_w$.

Accordingly, the ensemble of electrochemical and structural results shows $L_\alpha$ self-assembling patterns irrespectively of $\rho_{eff}$ values, while the best compaction levels are obtained at $\rho_{eff} = 4$. Additionally, it is known that CDplexes must be positively charged ($\rho_{eff} > 1$), but with cationic vector content being as low as possible to diminish cytotoxicity. All these considerations point to $\rho_{eff} = 4$ as a potentially adequate charge ratio to carry on both the proteomic and TE studies.

Upon in contact with biological milieu, CDplexes will adsorb plasma proteins in a time-dependent manner. Most abundant proteins will bind to vector surface first and will be progressively substituted by proteins with high affinity for the surface of CDplexes. At the equilibrium (typically reached within 1 h exposure), the PC of CDplexes will be constituted by a longstanding protein layer referred to as the *hard corona* (HC), which will provide CDplexes with their biological identity, plus a *soft corona* (SC) made of proteins in dynamical exchange with the surrounding environment. In the present investigation, both paCDs and CDplexes were let to interact with HP for 1 h. The PC formation was confirmed by means of $\zeta$-potential and size measurements of the CDplexes in the absence and in the presence of HP. The data collected in Table 4 indicate that the bare complexes are positively charged ($\zeta$-potential around +30 mV), with mean hydrodynamic diameters of around 114 nm in the case of ADM70-pDNA CDplexes and around 150 nm for the other two CDplexes. After 1 h incubation with HP, a clear increase on the size of the complexes (hydrodynamic diameter increases around 40-45 nm in the three cases), and a marked drop in $\zeta$-potential, shifting from positive to negative (from ca. +30 mV to ca. −17 mV), were observed. These evidences are clearly compatible with the formation of a ca. 20-nm-thick PC, mostly consisting of negatively charged proteins (i.e. pI < 7), that are located

at the CDplex surface. It is also remarkable that **ADM70-pDNA** formulations, either in the absence or in the presence of HP, exhibited higher stability and homogeneity in size (in view of PdI values) as compared to **ADM105** and **PBO234** formulations.

**Table 4.** Hydrodynamic diameter ($D_h$), polydispersity index (*PdI*) and $\zeta$-potential values of ADM70-pDNA, ADM105-pDNA and PBO234-pDNA CDplexes formulated at $\rho_{eff}$ = 4 before and after exposure to HP for 1h.

| | $D_h$ (nm) | *PdI* | $\zeta$-potential (mV) |
|---|---|---|---|
| **ADM70**-pDNA | 114 ± 6 | 0.21 ± 0.01 | 29.8 ± 1.2 |
| **ADM70**-pDNA + HP | 153 ± 8 | 0.34 ± 0.03 | -17.4 ± 2.5 |
| **ADM105**-pDNA | 149 ± 15 | 0.41 ± 0.08 | 31.7 ± 2.2 |
| **ADM105**-pDNA+HP | 191 ± 18 | 0.64 ± 0.13 | -16.3 ± 2.5 |
| **PBO234**-pDNA | 155 ± 12 | 0.53 ± 0.09 | 28.4 ± 1.4 |
| **PBO234**-pDNA+ HP | 203 ± 28 | 0.66 ± 0.16 | -18 ± 7 |

NanoLC-MS/MS experiments were run with the aim of identifying the corona proteins of the Janus paCD-pDNA formulations herein studied upon incubation with HP. In the case of **PBO234** and **PBO234**-pDNA CDplexes, incubation with HP did produce a tightly bound PC that could not be solubilized within the concentration range according to the standard protocols, preventing any further analysis. For **ADM70** and **ADM105** formulations, the relative protein abundance (RPA) of all the identified corona proteins was determined. Tables S1 and S2 report the top 25 most abundant proteins found within the corona of **ADM70** and **ADM105**, respectively (in the absence and presence of pDNA). All the proteins constituting the corona and these top 25 most

abundant ones are classified by their molecular mass (MW) and their isoelectrical point (pI) in Fig. 5. In the absence of pDNA, **ADM70** PC is formed mostly by proteins with molecular weight between 60-80 kDa (RPA~23%) and 150-300 kDa (RPA~11%). In the PC of **ADM70**-pDNA CDplex, proteins between 60-80 kDa remains roughly the same (RPA~21%), while a slight decrease in high MW proteins (150-300 kDa, RPA from 11 to 8%) and an increase in those under 20 kDa (RPA from 7 to 11%) was observed. Experiments for **ADM105** show that proteins with a molecular weigh between 60-80 kDa have RPA~28%, irrespective of the absence or presence of pDNA, while the RPA for proteins with MW 150-300 kDa increases from ~8% for **ADM105** to 14% for **ADM105**-pDNA CDplexes. For both cyclodextrin-based vectors, with and without pDNA, the corona is made up of proteins with a pI between 5 and 6 (33% for **ADM70** and 44% for **ADM105**), meaning that the adsorbed proteins have mostly a negative charge (pI < 7), in total agreement with the zeta potential results above commented. These results are in concordance with the idea that electrostatic intermolecular forces drive the non-covalent interaction between proteins and the cationic vectors.

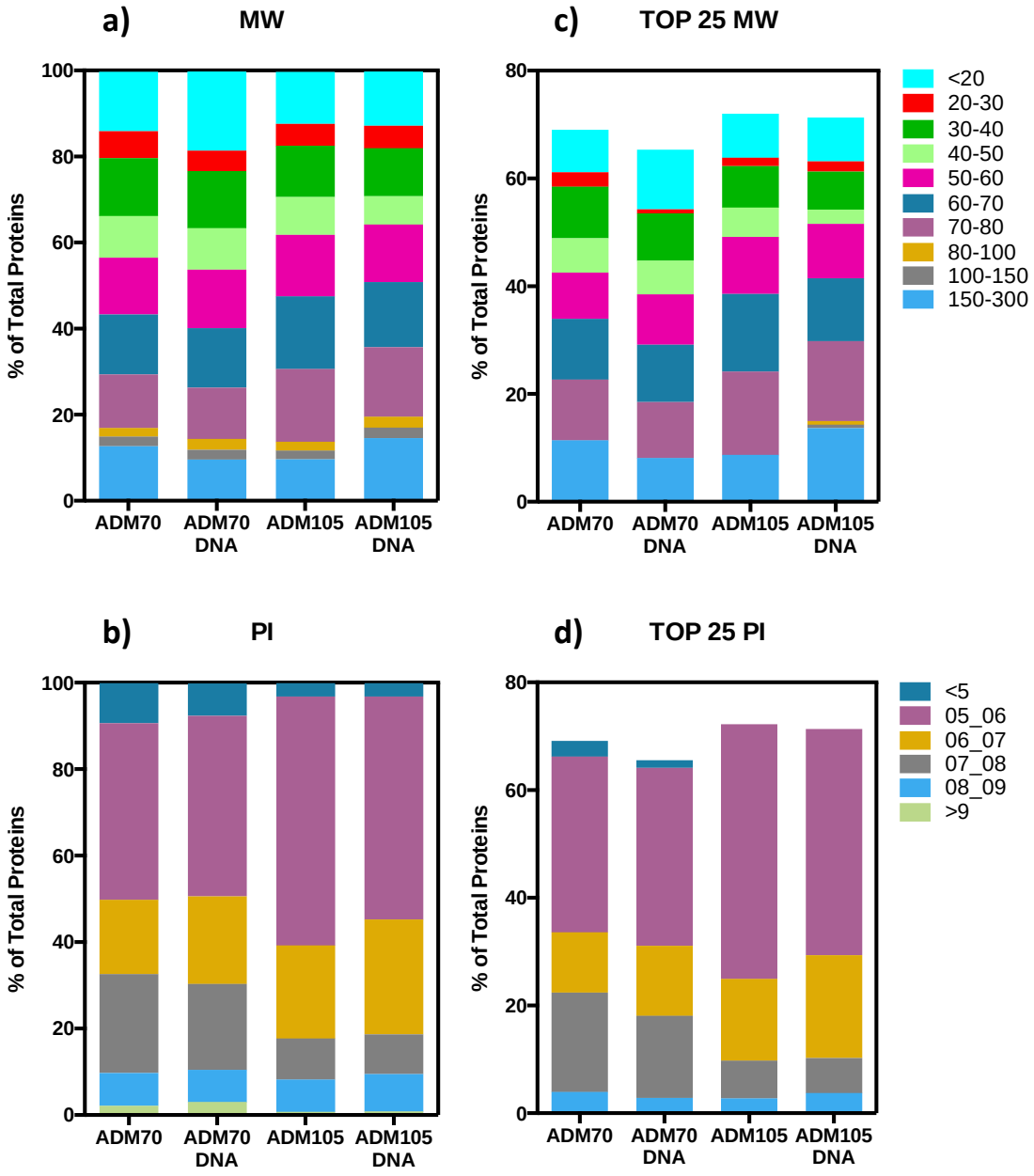


**Fig. 5.** Percentage of total proteins of corona proteins of **ADM70** and **ADM105** in the absence and presence of pDNA, classified according to their calculated molecular mass, MW (a), and isoelectric point, *pI* (b). Percentage of total proteins of the top 25 corona proteins classified according to their calculated molecular mass, *MW* (c) and isoelectric point, *pI* (d). Percentage of total proteins was calculated as explained in the experimental section.

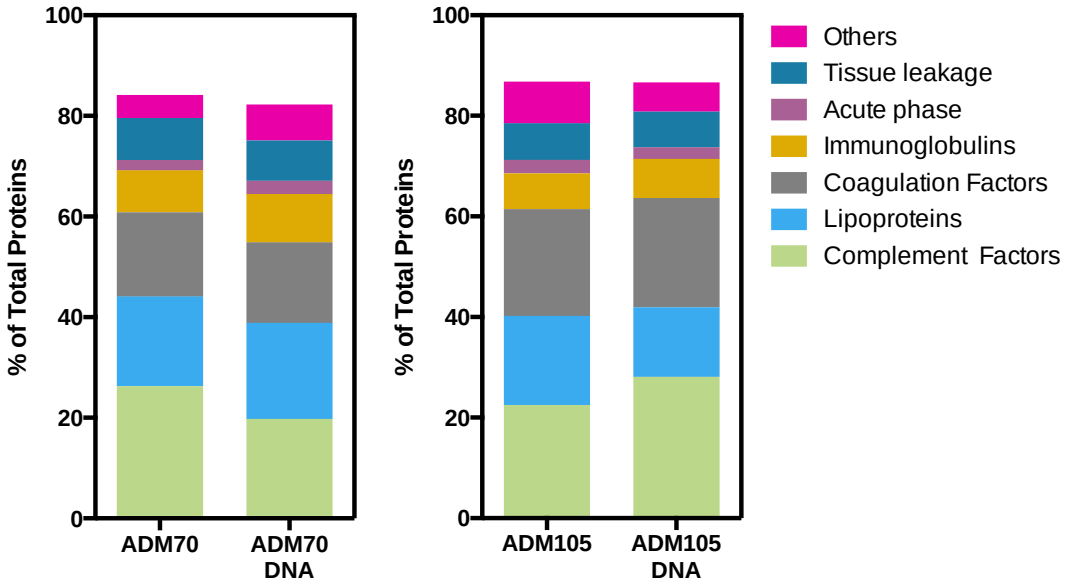


**Fig. 6.** Percentage of the proteins found within the protein corona (PC) of **ADM70** and **ADM105**, in the absence and presence of pDNA, classified by their physiological functions.

Corona proteins are also classified by their physiological functions (Fig. 6). For **ADM70** and **ADM105** nanoaggregates and for the corresponding CDplexes, complement, lipoprotein and coagulation were found to be the most abundant proteins, whereas immunoglobulins, tissue leakage and acute phase proteins constituted a minor fraction of the PC. Complement proteins promote elimination from systemic circulation, accumulation in the liver, spleen and clearance, and they are involved in immune response. Coagulation proteins are involved in coagulation processes, whereas lipoproteins affect the intracellular trafficking. Figs. S2 and S3 report a bioinformatic classification of corona proteins, in terms of percentage of total proteins identified for each functional class. As can be inferred from those plots, prothrombin presents the highest percentage for both paCDs in the absence of pDNA, followed by C4BPA, vitronectin, albumin and APOA1. In the case of the CDplexes, the trend is very similar, although the abundance of albumin is more affected by the type of paCD and/or the absence/presence of pDNA. It is worthwhile mentioning that prothrombin is involved in

coagulation process, C4BPA controls the activation of complement classical pathway, vitronectin is a receptor for cancer cells, albumin promotes prolonged blood circulation and crossing biological barriers, while APOA1 is the major protein of high density lipoproteins (HDL) and can be used as a ligand.

Lastly, transfection efficiency (TE) and cell viability of Janus paCD-based CDplexes have been evaluated in HeLa and MCF-7 cancer cells at $\rho_{eff}$ = 4 in the absence and presence of Human Plasma (HP). Lipofectamine was used as a positive control. In Fig. 7, TE results are reported in terms of % GFP expressed (panels a-b) and mean fluorescence intensity (MFI) (panels c-d). High values of % GFP indicate that there is a significant percentage of cell population expressing GFP protein, while a high MFI value points to a high level of GFP protein expression per cell that results from the number of copies of pDNA transfected, transcripted and translated per cell. Efficient transfection reagents often suffer, nonetheless, from high cytotoxicity. To evaluate whether or not Janus paCD formulations were toxic, HeLa and MCF-7 cancer cells were treated with the corresponding CDplexes and then subjected to MTT analysis, whose results are resumed in Fig. 8. Notably, Fig. 7 shows that CDplexes formulated at $\rho_{eff}$ = 4 transfect the cells roughly as poorly efficiently as the control, in terms of MFI, or slightly worst, in what respect to %GFP. Nonetheless, cell viability outputs were reasonably good (70 - 100%) at this $\rho_{eff}$, both in absence and in presence of HP (Fig. 8).

In an attempt to overcome such poor TE results, two strategies were designed: i) we increased the concentration of CDplexes/cell, but keeping $\rho_{eff}$ = 4, since recent results [58] point to this increase as a favorable factor to improve TE performances; and/or ii) we increased $\rho_{eff}$, with the risk of increasing cytoxicity levels as well. Fig. S4 shows the results obtained working with the first approach. As can be seen, increasing the CDplexes concentration per cell (2X, 5X and even 10X) yield transfection efficiencies

even lower than those previously obtained (1X), in contrast with the standard Lipofectamine for which an increase in the CDplexes doses provokes a clear improvement on TE results for HeLa cells. Furthermore, cytoxicity levels show a slight increase when CDplexes/cell concentration is raised for both the samples and the control. This non desirable combination (decrease on TE and increase on cytotoxicity) clearly reveals that the first strategy must be discarded for the CDplexes herein reported.

Fig. 7 shows the results obtained with the second approach, i.e. increasing $\rho_{eff}$ up to 25 and 50, together with those corresponding to $\rho_{eff} = 4$, previously commented. As can be seen, the three paCDs were more efficient transfecting pDNA than Lipofectamine (better %GFP and MFI values) at these higher $\rho_{eff}$, both in the absence and in the presence of HP. In the absence of HP and at high $\rho_{eff}$, MFI results (Fig. 7 c-d) followed the trend **ADM70**-pDNA ≈ **ADM105**-pDNA > **PBO234**-pDNA, irrespective of the cell line, although the superiority of **ADMs** were more evident in MCF-7 cells. However, certain reduction in transfection efficiency promoted by the presence of HP was found, a feature that could be due to a reduced endosomal escape in the cytoplasm of cells. Indeed, while HP can promote interaction with cell receptors, fusion with endosomal membranes could be, at least in part, impaired by the rich protein layer adsorbed at the surface of the vector. Nonetheless, some proteins forming the corona could shuttle the complex to acid cell compartments (e.g. lysosomes) where the gene payload could be degraded. In spite of the reduction on TE outcomes provoked by the presence of HP, CDplexes consisting of **ADMs**, and in particular PC-coated **ADM70**-pDNA CDplexes, produced again better MFI values (primarily for MCF-7 cells), suggesting that, although the PC is probably detrimental for cell uptake, the intracellular steps leading

to protein expression, including endosome scape, trafficking to the nucleus and pDNA release, are particularly favorable for PC-coated ADM70-pDNA CDplexes.

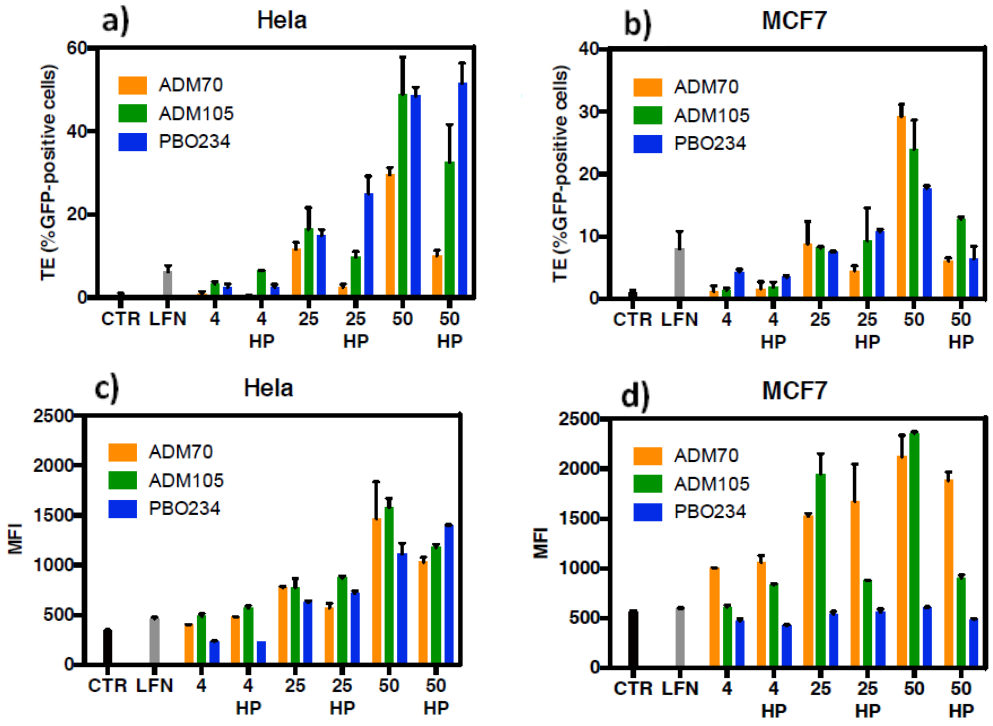


**Fig.7.** Transfection efficiency (TE) values of paCDs-pDNA CDplexes, in terms of % GFP expressed (panels a-b) and mean fluorescence intensity (MFI) (panels c-d), at $\rho_{eff}$ = 4, 25 and 50, in the absence and presence of Human Plasma (HP), through HeLa and MCF-7 cells. CTR: cells alone. LFN: Lipofectamine, positive control.

On the other hand, as shown in Fig. 8, the increase on effective charge ratio ($\rho_{eff}$) from 4 to 50 seems to slightly decrease the viability of HeLa cells, in the absence of HP, while no appreciable decrease is observed in MCF-7 cells. In the presence of PC, cell viability of both cell lines was not appreciably diminished. Notice, nonetheless, that almost all the values are around or over 80%, which is considered a minimum threshold value. However, interpretation of the effect of PC on the cell viability of CDplexes must be done with caution. Whether PC reduce cell viability or protect the cells can be due to specific PC composition and, in turn, to the complex relationship between PC composition and nanocarrier processing by cell machinery [59]. Moreover, in the

absence of *in vivo* experiments, the evaluation of PC composition, although implies an important improvement with respect to the use of SDS PAGE experiments alone, does not allow one to depict strong conclusions about future *in vivo* applications (i.e. targeting ability, bio-distribution, cytotoxicity). In fact, in the literature, major works are discussing about mapping protein binding sites across the PC surface. In the absence of this piece of information, discussion about the potential role of corona proteins should be made, but kept at a minimum, as done in this work. Otherwise, the risk of speculation may be too high.

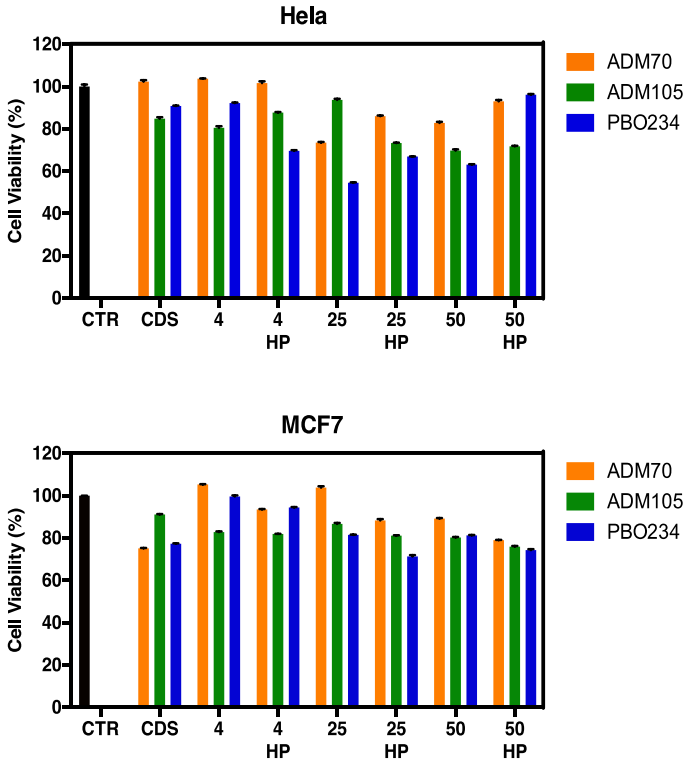


**Fig. 8.** Cell viability of paCDS-pDNA CDplexes at $\rho_{eff}$ = 4, 25 and 50 for HeLa and MCF-7 cells, in the absence and presence of human plasma (HP). CTR: cells alone. CDS: cells in the presence of paCDS without pDNA.

The above presented experimental evidences support that the Janus paCD structures ADM70 and ADM105 are promising nonviral vectors for pDNA delivery, overall

superior to PBO234 and to the Lipofectamine control. Differences in transfection efficiency as a function of the cell line might arise from differences in the preferred internalization routes. Thus, it has been reported that CDplexes can enter the cell by caveolae- and clathrin-mediated endocytosis, but only the first mechanism is productive regarding protein expression [30]. Moreover, CDplexes obtained from **ADM70** seem to exhibit the most favourable features for *in vitro* gene therapy applications: high stability in the absence or presence of HP, homogeneous size distribution, lower impact (with respect to the other two paCDs) of the PC in the capacity of the CDplexes to efficiently mediate protein expression *in cellulo*, and very low cytotoxicity even at high $\rho_{eff}$ values, and independently of the presence or not of HP. These features are in agreement with the previously observed superiority of **ADM70** formulations in *in vivo* transfection studies [33,34]. The body of biophysical and biochemical evidences obtained in this work provides a pathway for the rigorous characterization of pDNA-molecular vector formulations in view of their optimization for gene therapy applications. Broadening the current database on vector structures, electrochemical and structural properties of their aggregates, protein corona composition and transfection efficiencies in different *in vitro* and *in vivo* experimental settings should fund the basis for the rational design of second generation candidates. Work in that direction is currently sought in our laboratories.

## 4. Conclusions

This work was aimed to provide new insights in the fascinating processes governing pDNA complexation by monodisperse vectors of the Janus paCD family, in an attempt to delineate the mechanisms whereby differences in molecular structure translates into differences in transfection capabilities. For that purpose, three Janus CD-based

compounds (**ADM70**, **ADM105** and **PBO234**) have been thoroughly checked as potential nanocarriers of a pEGFP-C3 plasmid that codes for GFP expression to the interior of HeLa and MCF-7 cancer cells, both in the absence and presence of human serum. In a first level of organization, the vector molecular structure influences the effective positive charge available for interacting with the plasmid as well as the effective negative charge of the plasmid in the nanoaggregates. In fact, zeta potential study revealed that effective charges are lower than nominal ones both for the CD-based vectors (around 30% for ADMs and 25% for PBO234), and also for the pDNA, which renders a low percentage of its negative charge (less than 15%) when it is compacted by the nanocarriers. This is a potentially favourable finding since the weaker the anionic character of the DNA, the lower the amount of cationic vector needed to formulate the nanocomplexes, thus decreasing the cytotoxicity of the vector and increasing their potential output as safe and effective vehicles of nucleic acids. On the other hand, SAXS and cryo-TEM studies have shown that **ADM70**-pDNA, **ADM105**-pDNA and **PBO234**-pDNA CDplexes are structured according to a multilamellar lyotropic liquid crystal phase ($L_\alpha$). Two different multilamellar phases are distinguished, nonetheless, on cryo-TEM micrographs (CT-type and FP-type nanoaggregates), in coexistence with unilamellar vesicles of self-aggregated exceeding paCDs without pDNA compacted. Although the Janus feature seems to warrant a multilamellar arrangement for the paCD-pDNA nanocomplexes in all cases, their stability and homogeneity can be significantly different depending on the topology of the multivalent cationizable domain in the paCD entity. In the presence of human plasma, a second level of organization takes place involving the interaction with serum proteins, giving rise to multicomponent nanoassemblies equipped with a protein corona whose composition varies from a paCD formulation to another. The protein corona

(PC) characterization has also driven to interesting conclusions. The adsorbed proteins have mostly a negative charge in all the cases (pI < 7), pointing to the electrostatic interactions as the driven non-covalent forces between proteins and the cationic vectors. Complement, lipoprotein and coagulation were found to be the most abundant types of proteins within the corona of the Janus paCDs and the corresponding CDplexes, whereas immunoglobulins, tissue leakage and acute phase proteins constituted a minor fraction of the PC. At moderate-to-high charge ratios ($\rho_{eff}$ = 25 and 50), the bare CDplexes herein reported seem to transfect either HeLa or MCF-7 cancer cells more efficiently than Lipofectamine, and with high cell viabilities ranged from 80 to 100%. These transfection efficiencies were found to slightly decrease in the presence of biological media (HP), but in any case the values found were higher than those obtained with the control Lipofectamine. However, the effect of PC on the cell viability of CDplexes is not that easy to interpret. Probably, the specific PC composition and, in turn, its complex effect on nanocarrier processing by cell machinery, play a crucial role, although an accurate mapping of protein binding sites in the PC would be necessary to go further in these conclusions. In any case, the whole body of both biophysical and biochemical evidences obtained in this work allow us to conclude that the three paCDs proposed can be considered as potentially efficient nanocarriers *in vitro* and promising gen vectors for *in vivo* applications. Going further, among the three Janus paCDS nanovectors checked in this work, **ADM70** seem to exhibit the most favourable features for *in vitro* gene therapy applications requiring serum-containing media, in total agreement with the already observed superiority of **ADM70** formulations in *in vivo* transfection studies.

## Acknowledgments

MINECO of Spain, (contract numbers CTQ2012-30821, SAF2013-44021-R and CTQ2015-64425-C2-1-R), the Junta de Andalucía (contract number FQM2012-1467), University Complutense of Madrid (Spain) (project no. UCMA05-33-010) and the European Regional Development Funds (FEDER and FSE) for financial support. SAXS experiments were performed at NCD11 beamline at ALBA Synchrotron Light Facility with the collaboration of ALBA staff. Authors also thank C. Aicart-Ramos for carrying on amplification of plasmid DNA at the Departamento de Bioquímica y Biología Molecular I (UCM, Spain) and also P. Castro-Hartmann, Servei de Microscopia of UAB (Spain), for cryo-TEM experiments.

## Appendix A: Supplementary data

Supplementary Information available: Additional cryo-TEM micrographs, details and tables of the top 25 most abundant proteins in the protein corona of the CDplexes, and additional TE and cell viability experiments at higher CDplexes concentrations per cell. This information can be found on line at http://dx.doi.org/

## References

[1] E. Junquera, E. Aicart, Recent progress in gene therapy to deliver nucleic acids with multivalent cationic vectors, Adv. Colloid Interface Sci., 233 (2016) 161-175.
[2] I.M. Verma, M.D. Weitzman, Gene therapy: Twenty-first century medicine, Annu. Rev. Biochem., 74 (2005) 711-738.
[3] E. Junquera, E. Aicart, Cationic lipids as transfecting agents of DNA in gene therapy, Curr. Topics Med. Chem., 14 (2014) 649-663.
[4] T. Montier, T. Benvegnu, P.A. Jaffres, J.J. Yaouanc, P. Lehn, Progress in cationic lipid-mediated gene transfection: A series of bio-inspired lipids as an example, Curr. Gene Ther., 8 (2008) 296-312.
[5] R.S. Dias, B. Lindman, DNA Interaction with Polymers and Surfactants, Wiley & Sons, Hoboken, NJ, 2008.
[6] K. Ewert, N.L. Slack, A. Ahmad, H.M. Evans, A.J. Lin, C.E. Samuel, C.R. Safinya, Cationic lipid-DNA complexes for gene therapy: Understanding the relationship between complex structure and gene delivery pathways at the molecular level, Curr. Med. Chem., 11 (2004) 133-149.

[7] P.P. Karmali, A. Chaudhuri, Cationic liposomes as non-viral carriers of gene medicines: Resolved issues, open questions, and future promises, Med. Res. Rev., 27 (2007) 696-722.
[8] A.J. Kirby, P. Camilleri, J. Engberts, M.C. Feiters, R.J.M. Nolte, O. Soderman, M. Bergsma, P.C. Bell, M.L. Fielden, C.L.G. Rodriguez, P. Guedat, A. Kremer, C. McGregor, C. Perrin, G. Ronsin, M.C.P. van Eijk, Gemini surfactants: New synthetic vectors for gene transfection, Angew. Chem., Int. Ed., 42 (2003) 1448-1457.
[9] P. Kesharwani, V. Gajbhiye, N.K. Jain, A review of nanocarriers for the delivery of small interfering RNA, Biomaterials, 33 (2012) 7138-7150.
[10] B. Khurana, A.K. Goyal, A. Budhiraja, D. Arora, S.P. Vyas, siRNA delivery using nanocarriers - An efficient tool for gene silencing, Curr. Gene Ther., 10 (2010) 139-155.
[11] M.A. Islam, T.E. Park, B. Singh, S. Maharjan, J. Firdous, M.H. Cho, S.K. Kang, C.H. Yun, Y.J. Choi, C.S. Cho, Major degradable polycations as carriers for DNA and siRNA, J. Controlled Release, 193 (2014) 74-89.
[12] V.D. Badwaik, E. Aicart, Y.A. Mondjinou, M.A. Johnson, V.D. Bowman, D.H. Thompson, Structure-property relationship for in vitro siRNA delivery performance of cationic 2-hydroxypropyl-β-cyclodextrin: PEG-PPG-PEG polyrotaxane vectors, Biomaterials, 84 (2016) 86-98.
[13] W. Kusser, Chemically modified nucleic acid aptamers for in vitro selections: evolving evolution, Rev. Molec. Biotechnol., 74 (2000) 27-38.
[14] B.E. Eaton, The joys of in vitro selection: chemically dressing oligonucleotides to satiate protein targets, Curr. Opin. Chem. Biol., 1 (1997) 10-16.
[15] I.S. Blagbrough, A.A. Metwally, siRNA and Gene Formulation for Efficient Gene Therapy, InTech, 2013.
[16] C.E. Thomas, A. Ehrhardt, M.A. Kay, Progress and problems with the use of viral vectors for gene therapy, Nature Rev. Gen., 4 (2003) 346-358.
[17] P.D. Robbins, S.C. Ghivizzani, Viral vectors for gene therapy, Pharmacol Therapeut., 80 (1998) 35-47.
[18] M.A. Mintzer, E.E. Simanek, Nonviral vectors for gene delivery, Chem. Rev., 109 (2008) 259-302.
[19] K. Kumar, A.L. Barran-Berdon, S. Datta, M. Munoz-Ubeda, C. Aicart-Ramos, P. Kondaiah, E. Junquera, S. Bhattacharya, E. Aicart, A delocalizable cationic headgroup together with an oligo-oxyethylene spacer in gemini cationic lipids improves their biological activity as vectors of plasmid DNA, J. Mater. Chem. B, 3 (2015) 1495-1506.
[20] A.L. Barran-Berdon, S.K. Misra, S. Datta, M. Muñoz-Ubeda, P. Kondaiah, E. Junquera, S. Bhattacharya, E. Aicart, Cationic gemini lipids containing polyoxyethylene spacers as improved transfecting agents of plasmid DNA in cancer cells, J. Mater. Chem. B, 2 (2014) 4640-4652.
[21] D. Putnam, Polymers for gene delivery across length scales, Nature Mater., 5 (2006) 439-451.
[22] D.J. Bharali, I. Klejbor, E.K. Stachowiak, P. Dutta, I. Roy, N. Kaur, E.J. Bergey, P.N. Prasad, M.K. Stachowiak, Organically modified silica nanoparticles: A nonviral vector for in vivo gene delivery and expression in the brain, PNAS, 102 (2005) 11539-11544.
[23] C. Ortiz Mellet, J.M. Garcia Fernandez, J.M. Benito, Glycotransporters for gene delivery, in: A.P. Rauter, T.K. Lindhorst (Eds.) Carbohydrate Chemistry: Chemical and Biological Approaches vol. 38, 2012, pp. 338-375.

[24] C. Ortiz Mellet, J.M. Benito, J.M. García Fernandez, Preorganized, macromolecular, gene-delivery systems, Chem. Eur. J, 16 (2010) 6728-6742.
[25] Y. Aoyama, Macrocyclic glycoclusters: From amphiphiles through nanoparticles to glycoviruses, Chem. Eur. J, 10 (2004) 588-593.
[26] V. Bagnacani, V. Franceschi, M. Bassi, M. Lomazzi, G. Donofrio, F. Sansone, A. Casnati, R. Ungaro, Arginine clustering on calix-4-arene macrocycles for improved cell penetration and DNA delivery, Nature Commun., 4 (2013).
[27] J.L. Jiménez Blanco, F. Ortega-Caballero, L. Blanco-Fernández, T. Carmona, G. Marcelo, M. Martínez-Negro, E. Aicart, E. Junquera, F. Mendicuti, C. Tros de Ilarduya, C. Ortiz Mellet, J.M. García Fernández, Trehalose-based Janus cyclooligosaccharides: the ‘‘click’’ synthesis and DNA-directed assembly into pH-sensitive transfectious nanoparticles., Chem. Commun., 52 (2016) 10117-10120.
[28] S. Loethen, J.M. Kim, D.H. Thompson, Biomedical applications of cyclodextrin based polyrotaxanes, Polymer Reviews, 47 (2007) 383-418.
[29] C. Ortiz Mellet, J.M. García Fernandez, J.M. Benito, Cyclodextrin-based gene delivery systems, Chem. Soc. Rev., 40 (2011) 1586-1608.
[30] A. Diaz-Moscoso, D. Vercauteren, J. Rejman, J.M. Benito, C. Ortiz Mellet, S.C. De Smedt, J.M. García Fernandez, Insights in cellular uptake mechanisms of pDNA-polycationic amphiphilic cyclodextrin nanoparticles (CDplexes), J. Controlled Release, 143 (2010) 318-325.
[31] A. McMahon, E. Gomez, R. Donohue, D. Forde, R. Darcy, C.M. O'Driscoll, Cyclodextrin gene vectors: cell trafficking and the influence of lipophilic chain length, J. Drug Deliv. Sci. Technol., 18 (2008) 303-307.
[32] G. Caracciolo, H. Amenitsch, Cationic liposome/DNA complexes: from structure to interactions with cellular membranes, Eur. Biophys. J., 41 (2012) 815-829.
[33] C. Aranda, K. Urbiola, A.M. Ardoy, J.M. García Fernandez, C. Ortiz Mellet, C. Tros de Ilarduya, Targeted gene delivery by new folate-polycationic amphiphilic cyclodextrin-DNA nanocomplexes in vitro and in vivo, Eur. J. Pharm. Biopharm., 85 (2013) 390-397.
[34] A. Mendez-Ardoy, K. Urbiola, C. Aranda, C. Ortiz Mellet, J.M. Garcia Fernandez, C. Tros de Ilarduya, Polycationic amphiphilic cyclodextrin-based nanoparticles for therapeutic gene delivery, Nanomedicine, 6 (2011) 1697-1707.
[35] S.D. Wettig, R.E. Verrall, M. Foldvari, Gemini surfactants: A new family of building blocks for non-viral gene delivery systems, Curr. Gene Ther., 8 (2008) 9-23.
[36] P.C. Bell, M. Bergsma, I.P. Dolbnya, W. Bras, M.C.A. Stuart, A.E. Rowan, M.C. Feiters, J. Engberts, Transfection mediated by gemini surfactants: Engineered escape from the endosomal compartment, J. Am. Chem. Soc., 125 (2003) 1551-1558.
[37] A.L. Barran-Berdon, D. Pozzi, G. Caracciolo, A.L. Capriotti, G. Caruso, C. Cavaliere, A. Riccioli, S. Palchetti, A. Lagana, Time evolution of nanoparticle-protein corona in human plasma: Relevance for targeted drug delivery, Langmuir, 29 (2013) 6485-6494.
[38] D. Walczyk, F.B. Bombelli, M.P. Monopoli, I. Lynch, K.A. Dawson, What the cell “sees” in bionanoscience, J. Am. Chem. Soc., 132 (2010) 5761-5768.
[39] G. Caracciolo, F. Cardarelli, D. Pozzi, F. Salomone, G. Maccari, G. Bardi, A.L. Capriotti, C. Cavaliere, M. Papi, A. Lagana, Selective targeting capability acquired with a protein corona adsorbed on the surface of 1,2-dioleoyl-3-trimethylammonium propane/DNA nanoparticles, ACS Appl. Mater. Interfaces, 5 (2013) 13171-13179.

[40] G. Caracciolo, S. Palchetti, V. Colapicchioni, L. Digiacomo, D. Pozzi, A.L. Capriotti, G. La Barbera, A. Laganà, Stealth effect of biomolecular corona on nanoparticle uptake by immune cells, Langmuir, 31 (2015) 10764-10773.
[41] M. Lundqvist, J. Stigler, T. Cedervall, T. Berggård, M.B. Flanagan, I. Lynch, G. Elia, K. Dawson, The evolution of the protein corona around nanoparticles: a test study, ACS Nano, 5 (2011) 7503-7509.
[42] A.L. Capriotti, G. Caracciolo, C. Cavaliere, P. Foglia, D. Pozzi, R. Samperi, A. Lagana, Do plasma proteins distinguish between liposomes of varying charge density?, J. Proteomics, 75 (2012) 1924-1932.
[43] J.D. Byrne, T. Betancourt, L. Brannon-Peppas, Active targeting schemes for nanoparticle systems in cancer therapeutics, Adv. Drug Delivery Rev., 60 (2008) 1615-1626.
[44] V. Mirshafiee, M. Mahmoudi, K. Lou, J. Cheng, M.L. Kraft, Protein corona significantly reduces active targeting yield, Chem. Commun., 49 (2013) 2557-2559.
[45] H. Amenitsch, G. Caracciolo, P. Foglia, V. Fuscoletti, P. Giansanti, C. Marianecci, D. Pozzi, A. Lagana, Existence of hybrid structures in cationic liposome/DNA complexes revealed by their interaction with plasma proteins, Colloids Surf. B, 82 (2011) 141-146.
[46] A.L. Capriotti, G. Caracciolo, G. Caruso, P. Foglia, D. Pozzi, R. Samperi, A. Lagana, DNA affects the composition of lipoplex protein corona: A proteomics approach, Proteomics, 11 (2011) 3349-3358.
[47] A. Diaz-Moscoso, L. Le Gourrierec, M. Gomez-Garcia, J.M. Benito, P. Balbuena, F. Ortega-Caballero, N. Guilloteau, C. Di Giorgio, P. Vierling, J. Defaye, C. Ortiz Mellet, J.M. García Fernandez, Polycationic amphiphilic cyclodextrins for gene delivery: synthesis and effect of structural modifications on plasmid DNA complex stability, cytotoxicity, and gene expression, Chem. Eur. J., 15 (2009) 12871-12888.
[48] A. Gadelle, J. Defaye, Selektive halogenierung von cyclomaltooligosacchariden in C6-position und synthese von Per (3, 6-anhydro) cyclomaltooligosacchariden, Angew. Chem., 103 (1991) 94-95.
[49] M. Gómez-García, J.M. Benito, D. Rodríguez-Lucena, J.-X. Yu, K. Chmurski, C. Ortiz Mellet, R. Gutiérrez Gallego, A. Maestre, J. Defaye, J.M. García Fernández, Probing secondary carbohydrate-protein interactions with highly dense cyclodextrin-centered heteroglycoclusters: the heterocluster effect, J. Am. Chem. Soc., 127 (2005) 7970-7971.
[50] Y. Aoyama, T. Kanamori, T. Nakai, T. Sasaki, S. Horiuchi, S. Sando, T. Niidome, Artificial viruses and their application to gene delivery. Size-controlled gene coating with glycocluster nanoparticles, J. Am. Chem. Soc., 125 (2003) 3455-3457.
[51] S.K. Misra, M. Muñoz-Ubeda, S. Datta, A.L. Barran-Berdon, C. Aicart-Ramos, P. Castro-Hartmann, P. Kondaiah, E. Junquera, S. Bhattacharya, E. Aicart, Effects of a delocalizable cation on the headgroup of gemini lipids on the lipoplex-type nano-aggregates directly formed from plasmid DNA, Biomacromolecules, 14 (2013) 3951-3963.
[52] M. Muñoz-Ubeda, S.K. Misra, A.L. Barran-Berdon, S. Datta, C. Aicart-Ramos, P. Castro-Hartmann, P. Kondaiah, E. Junquera, S. Bhattacharya, E. Aicart, How does the spacer length of cationic gemini lipids influence the lipoplex formation with plasmid DNA? Physicochemical and biochemical characterizations and their relevance in gene therapy, Biomacromolecules, 13 (2012) 3926-3937.
[53] M. Muñoz-Ubeda, S.K. Misra, A.L. Barran-Berdon, C. Aicart-Ramos, M.B. Sierra, J. Biswas, P. Kondaiah, E. Junquera, S. Bhattacharya, E. Aicart, Why is less

cationic lipid required to prepare lipoplexes from plasmid DNA than linear DNA in gene therapy?, J. Am. Chem. Soc., 133 (2011) 18014-18017.
[54] J. Bednar, C.L. Woodcock, Chromatin, Academic Press Inc, San Diego, CA, 1999.
[55] J. Dubochet, M. Adrian, J.J. Chang, J.C. Homo, J. Lepault, A.W. McDowall, P. Schultz, Cryo-electron microscopy of vitrified specimens, Q. Rev. Biophys., 21 (1988) 129-228.
[56] J. Dubochet, B. Zuber, M. Eltsov, C. Bouchet-Marquis, A. Al-Amoudi, F. Livolant, How to "read" a vitreous section, in: Methods Cell. Biol., vol. 79, 2007, pp. 385-406.
[57] A.L. Barran-Berdon, M. Muñoz-Ubeda, C. Aicart-Ramos, L. Perez, M.R. Infante, P. Castro-Hartmann, A. Martin-Molina, E. Aicart, E. Junquera, Ribbon-type and cluster-type lipoplexes constituted by a chiral lysine based cationic gemini lipid and plasmid DNA, Soft Matter, 8 (2012) 7368-7380.
[58] S. Palchetti, D. Pozzi, C. Marchini, A. Amici, C. Andreani, C. Bartolacci, L. Digiacomo, V. Gambini, F. Cardarelli, C. Di Rienzo, G. Peruzzi, H. Amenitsch, R. Palermo, I. Screpanti, G. Caracciolo, Manipulation of lipoplex concentration at the cell surface boosts transfection efficiency in hard-to-transfect cells, Nanomed. Nanotechnol, Biol. Med., (2016) in press, DOI: 10.1016/j.nano.2016.1008.1019.
[59] D. Maiolo, P. Del Pino, P. Metrangolo, W.J. Parak, F.B. Bombelli, Nanomedicine delivery: does protein corona route to the target or off road?, Nanomedicine, 10 (2015) 3231-3247.

## Highlights

- Effective charges (lower than nominal) potentially improve CDplexes transfection outputs.
- CDplexes show $L_\alpha$ multilamellar patterns, quite appropriate to interact with cellular membranes.
- When exposed to human plasma CDplexes are covered by a rich protein corona.
- Optimized CDplexes exhibit high TE and very low cytotoxicity in HeLa and MCF7 cancer cells.
- TE/cell viability outputs of optimized CDplexes overcome those of the standard Lipofectamine.

## Graphical Abstract